Journal of Beijing Institute of Technology, 2021, Vol. 30, Suppl.1

Observation and Compensation of Friction in a Pneumatic Servo Welding System

Bo Wang✉ and Tao Wang

(School of Automation, Beijing Institute of Technology, Beijing 100081, China)

Abstract: Pneumatic servo systems are affected by nonlinear factors, especially friction between the inner wall of the cylinder and the piston. The limit-cycle oscillation caused by friction can easily result in dead-zone nonlinearity in a pneumatic servo system, reducing the system performance and repeatability. In this study, the impact of friction, which has a negative influence on a pneumatic servo welding system, is effectively reduced by observing and compensating the friction. The system is treated as a pneumatic position/force servo system before and after contact between the welding gun electrodes. A reduced-order observer and a Kalman filter are applied to observe and estimate dynamic and static friction. Then friction is compensated by using feed-forward control. The experimental results show that a steady-state error of within 1.3% is achieved for a step signal.

Key words: friction; pneumatic servo welding system; reduced-order observer; Kalman filter

CLC number: TP273 **Document code:** A **Article ID:** 1004-0579(2021)S1-0103-08

Pneumatic servo systems are widely used in industrial applications because of their low cost, easy maintenance, clean environment and other advantages[1-5]. However, because of nonlinear factors, including the dead zone of the solenoid valve, the compressibility of the gas, and friction between the piston and the cylinder wall, it is difficult to achieve accurate servo control. In particular, friction seriously affects servo system stability[6-9]. The limit-cycle oscillation caused by friction can easily cause dead-zone nonlinearity in servo control systems, which can reduce the system resolution and repeatability. On the one hand, fluctuations in friction force cause non-uniform velocity. The conversion of static and dynamic friction will lead to the creep phenomenon at low speed. On the other hand, the influence of static friction leads to a difference between the output force of the cylinder and the pressure in the chamber. A certain error will be generated if the cylinder output force is calculated using the two chamber pressure values.

The negative effects of friction on pneumatic servo systems have been widely investigated[10-11]. Meng et al.[12] established a dynamic friction model for a cylinder based on the LuGre model. Using experimental data, Belforte[13] developed a formula describing the cylinder friction and changes in pressure for the two cavities and for the movement speed. Extending this research, Raparelli et al.[14-15] used a finite element model to analyze friction for the cylinder seal for the first time, and confirmed the stress state and friction force for a double O-type sealing ring under different lubrication conditions. Yukio et al.[16] investigated the creep phenomenon under two different driving circuits for concrete cylinders. However they all designed special experimental test benches to study the friction. The friction model is made by using experimental data offline, which has a large deviation from the actual situation.

Resistance spot welding is of significant im-

Received 2020-09-15
Supported by the National Natural Science Foundation of China(51375045)
✉ Author for correspondence, senior experimentalist, Ph.D.
E-mail: wangbo231@bit.edu.cn
DOI: 10.15918/j.jbit1004-0579.20121

portance in the automobile industry, since it accomplishes 90% of car body assembly. As the traditional air gun cannot change the electrode force by control valves during the welding process, a servo gun that can control the electrode force was developed[17-18]. Compared with an electric servo gun, the pneumatic servo gun has the advantages of low cost and easy maintenance. Although several well-known pneumatic component manufacturers such as SMC, FESTO and NORGREN, have developed commercial products, the characteristics of friction in the pneumatic servo gun have not yet studied.

A pneumatic servo welding gun system is studied in this paper. During welding, the welding electrodes approach the workpieces and then exert pressure after contact. Thus, we can regard two different systems when the electrodes are open and closed. We consider the system before electrode contact as a pneumatic position servo system and apply a reduced-order observer (ROO) to observe dynamic friction. We consider the system after electrode contact as a pneumatic force servo system and apply a Kalman filter to estimate static friction. Feed-forward compensation is applied to the dynamic and static friction forces to achieve high control precision and repeatability.

1 Pneumatic Servo System

1.1 System structure

A schematic of the pneumatic servo welding system is depicted in Fig. 1. The system consists of a cylinder, a welding gun, two proportional valves, a position sensor, a force sensor, two pressure sensors, a digital signal processor (DSP) and a PC. In this system, the output position and force are controlled by a force that arises from the pressure differential across the piston in the cylinder. Compressed air from the gas source enters the cylinder chambers via different proportional valves.

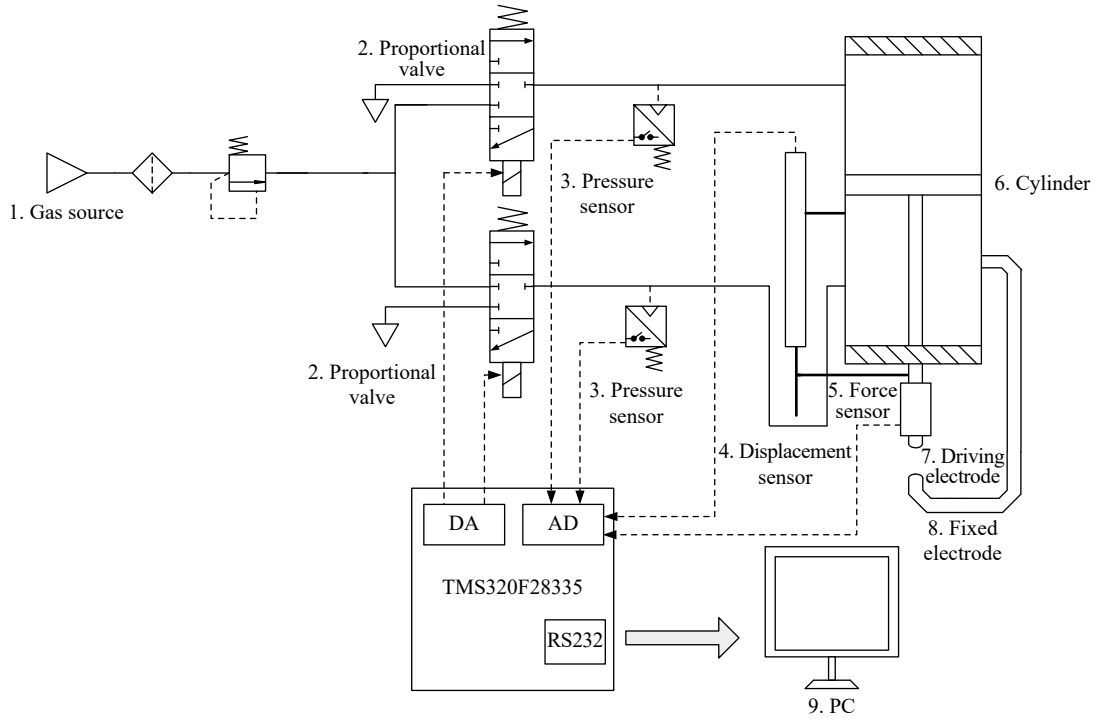

Fig. 1 Schematic diagram of the pneumatic servo welding system

1.2 System model

The pneumatic servo welding system that we consider is a cylinder system controlled by two proportional valves. The state and gas flow equations can be linearized for the midpoint of the cylinder balance position to obtain the balance

equations for flows into and out of the chambers without and with a rod[19].

$$\begin{cases} \dfrac{1}{RT_s}\left(p_{a0}A_a\dot{y}+\dfrac{V_{a0}}{k}\dot{p}_a\right)=k_1u+k_2p_a \\ \dfrac{1}{RT_s}\left(-p_{b0}A_b\dot{y}+\dfrac{V_{b0}}{k}\dot{p}_b\right)=k_3u+k_4p_b \end{cases} \tag{1}$$

where u is the control value; y is the piston rod displacement; R is the gas constant; T_s is the initial cavity temperature; p_a, A_a, p_{a0}, and V_{a0} are the pressure, force area, initial pressure and initial volume respectively, in the chamber without a rod; p_b, A_b, p_{b0}, and V_{b0} are the pressure, force area, initial pressure, and initial volume, respectively, in the chamber with a rod and k is an adiabatic coefficient. k_1, k_2, k_3 and k_4 are proportional coefficients for port flow through the proportional valves in the cylinder balance position after linearization.

The differential equation describing the piston and load dynamics is given by

$$p_aA_a-p_bA_b-F_f=M\ddot{y} \tag{2}$$

where M is the piston and rod assembly mass and F_f is the friction.

By applying the Laplace transform to Eqs. (1) (2), the mathematical model of the pneumatic servo welding system is obtained. The block diagram of the system mathematical model is shown in Fig. 2.

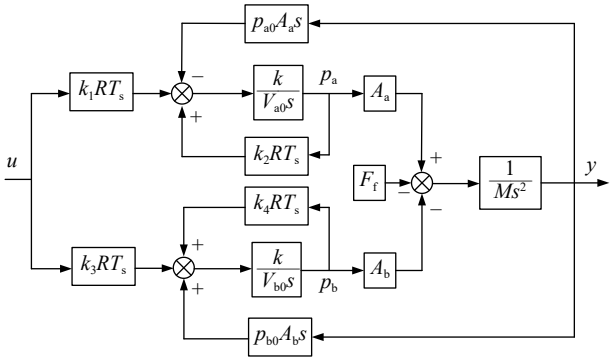

Fig. 2 Block diagram of the mathematical model for the system

The transfer function from input control to output position is

$$\frac{y(s)}{u(s)}=\frac{kRT_s(k_1A_aV_{b0}-k_3A_bV_{a0})}{MV_{a0}V_{b0}s^3+(k_2A_a^2p_{a0}V_{b0}+k_4A_b^2p_{b0}V_{a0})s} \tag{3}$$

By a system recognition method, the transfer functions from input control to output position in two stages of the forward and reverse processes can be obtained.

2 Observation and Estimation of the Friction

2.1 Stribeck friction model

The Stribeck friction model is widely used in pneumatic servo systems[20]. The Stribeck friction model is shown in Fig. 3.

The formula of the Stribeck friction model is

$$F_f=\begin{cases} F_c+(F_s-F_c)\,e^{-v/v_s}+k_vv, & v\neq 0 \\ F_e, & v=0 \quad \text{and} \quad |F_e|<F_s \\ F_s\text{sgn}\,(F_e), & v=0 \quad \text{and} \quad |F_e|\geq F_s \end{cases} \tag{4}$$

where F_c is the Coulomb friction; F_s is the maximum static friction; v_s is the Stribeck velocity; k_v is the viscous friction coefficient; F_e is the external force of the piston.

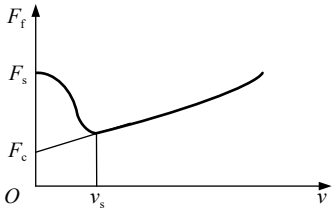

Fig. 3 Stribeck friction model

The Stribeck friction model is usually made by using experimental data offline and an experimental test bench is needed. However, the parameters of the Stribeck friction model are variable under different working conditions, meaning it is difficult to obtain a precise model of friction.

2.2 Observation of dynamic friction

As a result of machining and assembly variations, friction between the cylinder and the piston rod is not exactly the same for each cylinder. Dynamic friction in the cylinder at low speed will

have a serious impact on precise control of the position. To overcome the low-speed creep phenomenon and improve control precision, dynamic friction during piston motion is observed to realize real-time compensation. Since a position sensor is already used to detect the position of the piston, the ROO is used to observe dynamic friction on the piston.

The following state space is established by motion Eq. (2)

$$\begin{cases}\begin{bmatrix}\dot{v}\\ \dot{F}_{\mathrm{f}}\end{bmatrix}=\begin{bmatrix}0 & -\dfrac{1}{M}\\ 0 & 0\end{bmatrix}\begin{bmatrix}v\\ F_{\mathrm{f}}\end{bmatrix}+\begin{bmatrix}\dfrac{A_{\mathrm{a}}}{M}\\ 0\end{bmatrix}\left[p_{\mathrm{a}}-\dfrac{A_{\mathrm{b}}}{A_{\mathrm{a}}}p_{\mathrm{b}}\right]\\ v=[1\quad 0]\begin{bmatrix}v\\ F_{\mathrm{f}}\end{bmatrix}\end{cases}\tag{5}$$

where v is the velocity of the piston. v can be obtained by differentiating the position value measured by the position sensor.

$$\boldsymbol{A}=\begin{bmatrix}0 & -\dfrac{1}{M}\\ 0 & 0\end{bmatrix},\ \boldsymbol{B}=\begin{bmatrix}\dfrac{A_{\mathrm{a}}}{M}\\ 0\end{bmatrix},\ \boldsymbol{C}=[\,1\quad 0\,]$$

$$\operatorname{rank}\begin{bmatrix}\boldsymbol{C}\\ \boldsymbol{CA}\end{bmatrix}=2$$

Thus the system is observable.

To facilitate generalization of the derivation, we rewrite Eq. (5) as

$$\begin{cases}\begin{bmatrix}\dot{X}_1\\ \dot{X}_2\end{bmatrix}=\begin{bmatrix}A_{11} & A_{12}\\ A_{21} & A_{22}\end{bmatrix}\begin{bmatrix}X_1\\ X_2\end{bmatrix}+\begin{bmatrix}B_1\\ B_2\end{bmatrix}u\\ v=X_1\end{cases}\tag{6}$$

Then

$$\begin{cases}\dot{v}=A_{11}v+A_{12}X_2+B_1u\\ \dot{X}_2=A_{22}X_2+A_{21}v+B_2u\end{cases}\tag{7}$$

Define $\bar{u}=A_{21}v+B_2u$ and $w=\dot{v}-A_{11}v-B_1u$

$$\begin{cases}\dot{X}_2=A_{22}X_2+\bar{u}\\ w=A_{12}X_2\end{cases}\tag{8}$$

The ROO is

$$\dot{\hat{X}}_2=(A_{22}-LA_{12})\hat{X}_2+Lw+\bar{u}\tag{9}$$

where L is the feedback gain matrix of the state observer. L is obtained by the method of pole assignment.

To eliminate $\dot{v}$, we define $z=\hat{X}_2-Lv$

$$\begin{aligned}\dot{z}=&(A_{22}-LA_{12})z+[(A_{22}-LA_{12})L+\\ &(A_{21}-LA_{11})]v+(B_2-LB_1)u\end{aligned}\tag{10}$$

where $A_{11}=A_{21}=A_{22}=B_2=0$.

$$\dot{z}=-LA_{12}z-LA_{12}Lv-LB_1u\tag{11}$$

In the actual system, A_{a}=0.005 03 m², A_{b}= 0.004 54 m² and M=2 kg. Thus, A_{12} =−1/2 and B_1= 0.002 515.

In theory, the ROO can reconstruct the observation part in any fast speed, but is limited by noise and sensitivity in actual realization. After comprehensive evaluation, the observer pole is set to −50, so L=−100.

Substituting the actual parameters

$$\dot{z}=-50z+5\,000v+0.251\,5u\tag{12}$$

To obtain the transfer function for the dynamic friction formula, define $z=z_1+z_2$, then

$$\dot{z}=\dot{z}_1+\dot{z}_2$$

$$\dot{z}_1+\dot{z}_2=-50\,(z_1+z_2)+5\,000v+0.251\,5u$$

Define $\dot{z}_1=-50z_1+5\,000v$ and $\dot{z}_2=-50z_2+0.251\,5\ u$

Applying the Laplace transform

$$\begin{cases}z_1(s)=\dfrac{5\,000}{s+50}v(s)\\ z_2(s)=\dfrac{0.251\,5}{s+50}u(s)\end{cases}\tag{13}$$

For $\hat{F}_{\mathrm{f}}=\hat{X}_2=z+Lv$, the dynamic friction transfer function is

$$\begin{aligned}\widehat{F}_{\mathrm{f}}(s)=&z_1(s)+z_2(s)+Lv(s)=\\ &\frac{5\,000}{s+50}v(s)+\frac{0.251\,5}{s+50}u(s)-100v(s)\end{aligned}\tag{14}$$

2.3 Estimation of static friction

After electrode contact, we can only control the pressure in the chamber of the cylinder without the rod. The fixed electrode can be regarded as an infinite load. Thus, this movement process can be regarded as the piston not moving while the output force changes. At this point, static friction mainly acts. It is difficult to establish a state equation to observe static friction, so a Kalman filter is established to estimate the static friction.

Rewrite Eq. (5)

$$\begin{cases} \begin{bmatrix} \dot{F}_{\mathrm{f}} \\ \ddot{F}_{\mathrm{f}} \end{bmatrix} = \begin{bmatrix} 0 & 1 \\ 0 & 0 \end{bmatrix} \begin{bmatrix} F_{\mathrm{f}} \\ \dot{F}_{\mathrm{f}} \end{bmatrix} + W \\ F - p_{\mathrm{a}} A_{\mathrm{a}} = \begin{bmatrix} -1 & 0 \end{bmatrix} \begin{bmatrix} F_{\mathrm{f}} \\ \dot{F}_{\mathrm{f}} \end{bmatrix} + V \end{cases} \tag{15}$$

where F is the output force, W is process noise with covariance matrix Q, and V is observation noise with covariance matrix R. W and V are all uncorrelated white noise and their average is zero.

To facilitate the analysis, change Eq. (15) to the form

$$\begin{cases} \dot{X} = FX + Q \\ Y = CX + R \end{cases} \tag{16}$$

And discretization

$$\begin{cases} X(k) = AX(k-1) + Q(k) \\ Y(k) = CX(k) + R(k) \end{cases} \tag{17}$$

where $A = \mathrm{e}^{FT_{\mathrm{s}}}$. T_{s} is the sampling period.

The Kalman filtering recursive algorithm comprises the following five steps.

① Predict the state estimate

$$\hat{X}(k|k-1) = AX(k-1|k-1) \tag{18}$$

② Predict the estimate covariance

$$P(k|k-1) = AP(k-1|k-1)A^{\mathrm{T}} + Q(k-1) \tag{19}$$

③ Calculate the optimal Kalman gain

$$K_{\mathrm{g}}(k) = P(k|k-1)C^{\mathrm{T}}[CP(k|k-1)C^{\mathrm{T}} + R(k)]^{-1} \tag{20}$$

④ Update the state estimate

$$\hat{X}(k|k) = \hat{X}(k|k-1) + K_{\mathrm{g}}(k)[Y(k) - C\hat{X}(k|k-1)] \tag{21}$$

⑤ Update the estimate covariance

$$P(k|k) = [I - K_{\mathrm{g}}(k)C]P(k|k-1) \tag{22}$$

In actual use, the covariance matrices Q and R are set by a trial method.

3 Simulation

A diagram of the designed ROO is shown in Fig. 4. A PID controller is designed to generate sinusoidal motion for the piston rod. In order to compare the effect of ROO, the Stribeck friction model of the cylinder is employed. The parameters of the Stribeck friction model are obtained by special testing experiments.

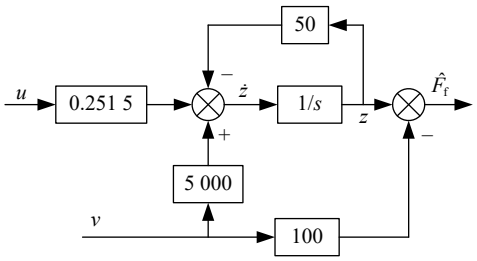

Fig. 4 Diagram of the reduced-order observer principle

The observation results for dynamic friction of the ROO are shown in Fig. 5. It can be seen that the ROO results closely fit the actual dynamic friction.

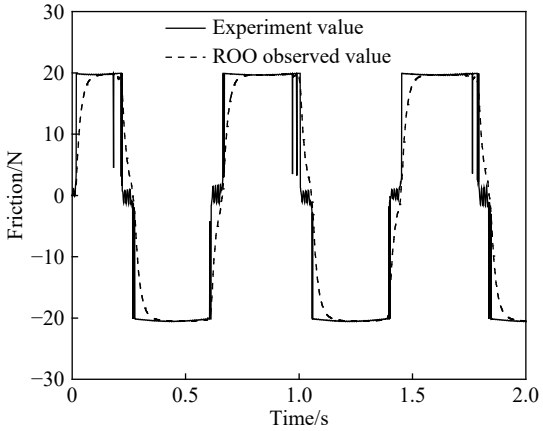

Fig. 5 Observation results for dynamic friction of ROO

4 Experiments and Discussion

4.1 Description of experimental test system

The experimental setup of the pneumatic servo welding gun system is depicted in Fig. 6. A booster cylinder (PNEUMAX 1321.80.25.80.60 HBSP) is selected as the actuator. This booster cylinder has three separate chambers. Here, we only use two of the chambers, which have a 60 mm stroke and a 80 mm diameter bore. Two proportional valves (SMC XT581-V-A) are used to control the charging and discharging process of both chambers of the cylinder. A linear variable differential transformer (LVDT) displacement sensor with a range of 50 mm is used to measure the position of the cylinder piston rod.

Two pressure sensors (SMC PSE540A) are also used in the setup for the measurement of two chamber pressures. A force sensor (NAICHUANG, CHINA FC-WM) with a range of 500 kg is used to measure the output force of the cylinder. The control and observer algorithms are implemented on a DSP system (TMS320F28335).

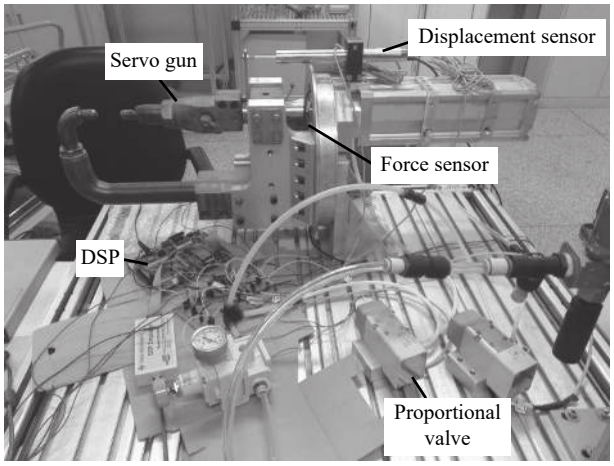

Fig. 6 Experimental setup of the pneumatic servo welding gun system

4.2 Before electrode contact

Write Eq. (14) in the form as follows

$$\begin{cases} F_1(s) = \dfrac{5\,000}{s+50} v(s) \\ F_2(s) = \dfrac{0.251\,5}{s+50} u(s) \\ \widehat{F}_{\mathrm{f}}(s) = F_1(s) + F_2(s) - 100v(s) \end{cases} \tag{23}$$

Eq. (23) is discretized to obtain the programming observer algorithm.

$$\begin{cases} F_1(k) = 0.67F_1(k-1) + 33.33v(k-1) \\ F_2(k) = 0.67F_2(k-1) + 1.67 \times 10^{-3} u(k-1) \\ F_{\mathrm{f}}(k) = F_1(k) + F_2(k) - 100v(k-1) \end{cases} \tag{24}$$

A feed-forward control, as shown in Fig. 7, is used to compensate the friction of the pneumatic cylinder. Here, u is the control voltage of the proportional valve. A compensating control value Δu is added to the input signal u. To realize compensation for dynamic friction, the value for $G_{\mathrm{f}}(s)$ needs to meet the equation $G_{\mathrm{f}}(s)G_1(s) = 1$. In order to calculate the compensating control value Δu, differentiation of the observed friction force is required. Δu is of the form $k_1 F_{\mathrm{f}}(k-1) + k_2 F_{\mathrm{f}}(k-2) + \cdots$. The coefficients can be obtained by practical experiments.

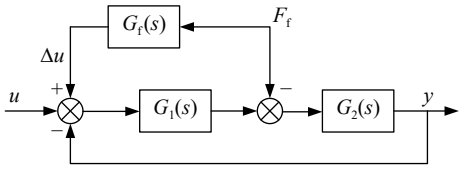

Fig. 7 Diagram of the compensation principle

First the pneumatic servo system is controlled by the PID control algorithm and the cylinder piston is subjected to sinusoidal tracking. The target sinusoidal signal is of a 6 mm amplitude and a 2 Hz frequency. The experimental results for the electrode displacement are shown in Fig. 8. It is evident from Fig. 8 that the cylinder is affected by dynamic friction during motion before compensation. The crawl phenomenon and hysteresis are clear. The friction needs to be compensated.

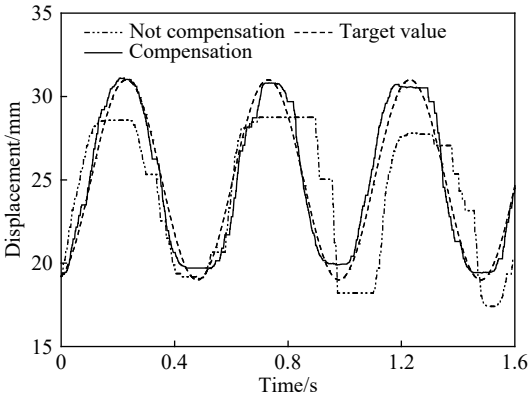

Fig. 8 Displacement results for sinusoidal responses

The results for dynamic friction compensation are shown in Fig. 8. The amplitude of the sinusoidal response target for the gun-driven electrode is 6 mm and the frequency is 2 Hz. It is clear that feed-forward compensation for the observed friction significantly improves the electrode displacement in comparison to a sinusoidal input signal by reducing both the response time and the steady-state error.

In order to compare the control effect of the proposed method, experiments for tracking step signals are also implemented. The experimental

results for position step response of 10, 20 and 30 mm are shown in Fig. 9. The results show that friction compensation effects the performance of the system largely. Without compensation, the steady-state error for displacement references of 10, 20 and 30 mm is 4%, 4% and 2.3%, respectively. After friction compensation, this error is reduced to less than 0.7%.

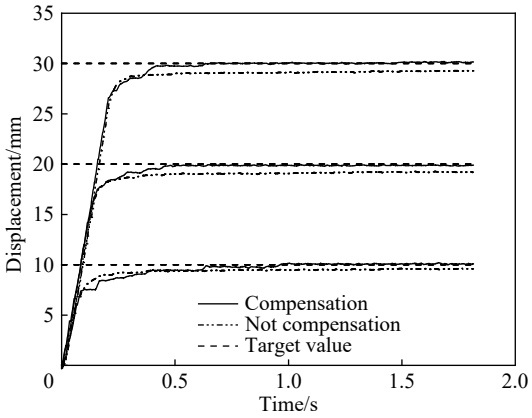

Fig. 9 Displacement results for step responses

4.3 After electrode contact

A Kalman filter is used to estimate the static friction after electrode contact. The friction compensation method is the same as for before electrode contact. The experimental results of a sinusoidal signal at 1 Hz and a 500 N amplitude are shown in Fig. 10. The results show that the output force essentially follows the target values after compensation for static friction.

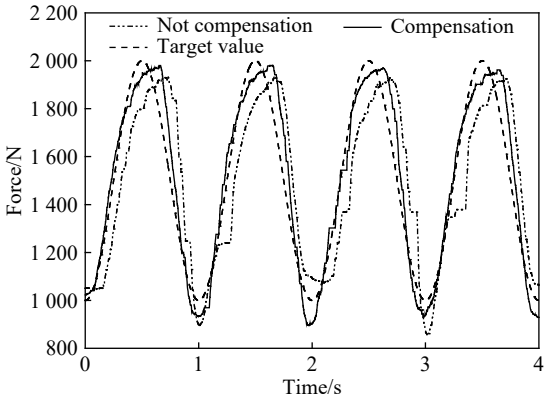

Fig. 10 Output force results for sinusoidal response

Experiments for tracking output force step signals are also implemented. The step signals are set to be 1500, 2000 and 2500 N. The step response of the system before and after static friction compensation is shown in Fig. 11. It is shown that compensation for static friction effectively reduces the steady-state error for the output force from 3%, 3%, and 3.2% to 1.3%, 0.5% and 0.8% for force steps of 1500, 2000 and 2500 N, respectively.

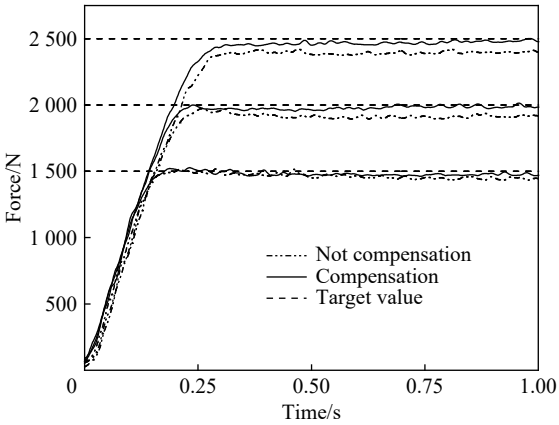

Fig. 11 Output force results for step response

5 Conclusion

The design of a ROO and a Kalman filter for a pneumatic servo welding system is presented. After the ROO and Kalman filter observe dynamic and static friction, a feed-forward control method is used to compensate the friction. The effectiveness of the proposed friction compensation method is demonstrated using experimental results. Improvements on this method can still be made. For example, time delay ineluctably appears in experiments when the frequency of a sinusoidal signal increased. The proposed method is very practical in pneumatic servo driving systems for resistance spot welding.

References:

[1] Lee L W, Li I H. Wavelet-based adaptive sliding-mode control with H-infinity tracking performance for pneumatic servo system position tracking control [J]. IET Control Theory and Applications, 2012, 6(11): 1699-1714.

[2] Kaitwanidvilai S, Olranthichachat P. Robust loop shaping-fuzzy gain scheduling control of a servo-pneumatic system using particle swarm optimiza-

tion approach [J]. Mechatronics, 2011, 21(1): 11-21.

[3] Saravanakumar D, Mohan B, Muthuramalingam T. Application of response surface methodology on finding influencing parameters in servo pneumatic system [J]. Measurement, 2014, 54: 40-50.

[4] Hodgson S, Tavaloli M, Pham M T, et al. Nonlinear discontinuous dynamics averaging and PWM-based sliding control of solenoid-valve pneumatic actuators [J]. IEEE/ASME Transactions on Mechatronics, 2015, 20(2): 876-888.

[5] Franco E, Rea M, Gedroyc W, et al. Control of a master-slave pneumatic system for teleoperated needle insertion in MRI [J]. IEEE/ASME Transactions on Mechatronics, 2016, 21(5): 2595-2600.

[6] Saleem A, Wong C B, Pu J, et al. Mixed-reality environment for frictional parameters identification in servo-pneumatic system [J]. Simulation Modelling Practice and Theory, 2009, 17(10): 1575-1586.

[7] Tsai Y C, Huang A C. Multiple-surface sliding controller design for pneumatic servo systems [J]. Mechatronics, 2008, 18(9): 506-512.

[8] Liu Y T, Kung T T, Chang K M, et al. Observer-based adaptive sliding mode control for pneumatic servo system [J]. Precision Engineering-Journal of the International Societies for Precision Engineering and Nanotechnology, 2013, 37(3): 522-530.

[9] Zhao L, Yang Y F, Xia Y Q, et al. Active disturbance rejection position control for a magnetic rodless pneumatic cylinder [J]. IEEE Transactions on Industrial Electronics, 2015, 62(9): 5838-5846.

[10] Li K, Zhang Y M, Wei S L, et al. Evolutionary algorithm-based friction feedforward compensation for a pneumatic rotary actuator [J]. Applied Sciences-Basel, 2018, 8(9): 1623.

[11] Carneiro J F, de Almeida F G. Friction characteristics and servo control of a linear peristaltic actuator [J]. International Journal of Advanced Manufacturing Technology, 2018, 96: 2117-2126.

[12] Meng D Y, Tao G L, Liu H, et al. Adaptive robust motion trajectory tracking control of pneumatic cylinders with LuGre model-based friction compensation [J]. Chinese Journal of Mechanical Engineering, 2014, 27(4): 802-815.

[13] Belforte G, Alfio N D, Raparelli T. Experimental analysis of friction force in pneumatic cylinders [J]. Journal of Fluid Control, 1989, 20(1): 42-60.

[14] Raparelli T, Bertettot A M, Mazzat L. Experimental and numerical study of friction in an elastomeric seal for pneumatic cylinders [J]. Tribology International, 1997, 30(7): 547-557.

[15] Belforte G, Raparelli T, Velardocchia M. Study of the behavior of lip seals in pneumatic actuators [J]. Lubrication Engineering, 1993, 49(10): 775-780.

[16] Terashima Y, Kawakami Y, Kawai S. A study on the effects of friction characteristics in pneumatic cylinder[C]// The Fourth International Symposium on Fluid Power Transmission and Control (ISFP'2003), Wuhan, China, 2003: 352-357.

[17] Zhang X Q, Chen G L, Zhang Y S. On-line evaluation of electrode wear by servo gun in resistance spot welding [J]. International Journal of Advanced Manufacturing Technology, 2008, 36(7): 681-688.

[18] Zhang X Y, Chen G L, Zhang Y S, et al. Improvement of resistance spot weld ability for dual-phase (DP600) steels using servo gun [J]. Journal of Materials Processing Technology, 2009, 209: 2671-2675.

[19] Hamiti K, Voda-Besancon A, Roux-Buisson H. Position control of a pneumatic actuator under the influence of stiction [J]. Control Engineering Practice, 1996, 4(8): 1079-1088.

[20] Armstrong B, Dupont P, Canudas de Wit C. A Survey of models, analysis tools and compensation methods for the control of machines with friction [J]. Automatica, 1994, 30(7): 1083-1138.